Differentiation of Intracranial Dural Metastases and Meningiomas Using DSC Perfusion MRI and Machine Learning

Seyit Erol *, Halil Özer, Ahmet Baytok, Ayşe Arı, Hakan Cebeci

Posted Date: 30 January 2026

doi: 10.20944/preprints202601.2266.v1

Keywords: dural metastases; meningioma; DSC perfusion MRI; machine learning

Article

Differentiation of Intracranial Dural Metastases and Meningiomas Using DSC Perfusion MRI and Machine Learning

Seyit Erol *, Halil Özer, Ahmet Baytok, Ayşe Arı and Hakan Cebeci

Department of Radiology, Selcuk University, Faculty of Medicine

Abstract

Objectives: To assess the diagnostic performance of dynamic susceptibility contrast (DSC) perfusion MRI parameters and machine learning methods for differentiating intracranial dural metastases from meningiomas. **Methods:** This retrospective diagnostic accuracy study included 56 patients (mean age, 57.6 ± 11.2 years; 20 men) with dural-based intracranial lesions, comprising 27 dural metastases and 38 meningiomas. All patients underwent DSC perfusion MRI. Relative cerebral blood volume (rCBV), relative cerebral blood flow (rCBF), diffusion metrics, and dynamic time–signal intensity curve parameters were extracted. Group comparisons were performed using nonparametric statistical tests. Machine learning models, including linear discriminant analysis (LDA), were developed using patient-level grouped nested cross-validation to avoid data leakage. Diagnostic performance was evaluated using out-of-fold receiver operating characteristic (ROC) analysis, calibration assessment, and clinically oriented thresholds prioritizing metastasis sensitivity. **Results:** rCBV_mean and rCBF_mean were significantly higher in meningiomas than in dural metastases (median rCBV_mean, 4.71 vs 2.95; median rCBF_mean, 3.44 vs 2.02; both $p < 0.001$). Diffusion metrics and dynamic perfusion parameters, including wash-in time, percentage signal recovery, and wash-out slope, did not differ significantly between groups ($p > 0.05$). Univariate ROC analysis demonstrated strong discrimination for both rCBF_mean (AUC, 0.82; 95% CI: 0.72, 0.90) and rCBV_mean (AUC, 0.82; 95% CI: 0.72, 0.91). An LDA model integrating rCBF_mean and rCBV_mean achieved an out-of-fold AUC of 0.81 (95% CI: 0.72, 0.89) and improved specificity (85%) at a fixed metastasis sensitivity of 85%. **Conclusion:** DSC perfusion MRI–derived rCBF and rCBV are robust biomarkers for differentiating intracranial dural metastases from meningiomas. An interpretable machine learning model integrating these parameters improves diagnostic specificity while maintaining high sensitivity.

Keywords: dural metastases; meningioma; DSC perfusion MRI; machine learning

1. Introduction

Differentiating intracranial dural metastases (IDM) from meningiomas poses a diagnostic challenge in neuroradiology due to their overlapping MRI features, such as dural-based enhancement and vasogenic edema [1,2]. Conventional MRI sometimes lacks the reliability to distinguish between the two, as their characteristic features like calcification in meningiomas and necrosis in metastases can overlap [3–5].

Perfusion-weighted MRI offers a potential solution by assessing tumor vascularity. Dynamic susceptibility contrast (DSC) MRI enables quantitative assessment of relative cerebral blood volume (rCBV) and relative cerebral blood flow (rCBF), parameters that have been extensively investigated in dural lesions [3,6]. While some studies have reported higher rCBV values in meningiomas compared to IDM [7] others have shown a significant overlap in rCBV measurements, particularly in hypervascular metastases [3].

 doi:10.20944/preprints202601.2266.v1

Beyond rCBV and rCBF, additional DSC-derived dynamic parameters, including wash-in and wash-out characteristics, have been explored to improve diagnostic performance. Shorter normalized wash-out times have been reported in IDM in some studies, whereas others found limited discriminatory value for dynamic perfusion or diffusion parameters such as apparent diffusion coefficient (ADC) [5,8].

Machine learning (ML) approaches provide a suitable framework for modeling complex, nonlinear relationships between quantitative biomarkers. By integrating DSC perfusion parameters within supervised classification models, ML has the potential to improve diagnostic accuracy while preserving clinical interpretability. Accordingly, the aim of this retrospective study is to evaluate the diagnostic value of DSC perfusion MRI parameters and to assess whether a simple ML-based model can enhance differentiation between IDM and meningiomas in a clinically applicable manner.

2. Materials and Methods

This retrospective study was approved by the local institutional review board (2024/541), and the requirement for informed consent was waived due to the retrospective study design, in accordance with the Declaration of Helsinki.

2.1. Statistical Analysis

Categorical variables were summarized as frequencies and percentages, and comparisons between groups were conducted using the chi-square test. For continuous variables, means, standard deviations, and 95% CIs were calculated. Continuous variables were assessed for normality using the Shapiro–Wilk test. As most parameters did not follow a normal distribution, continuous data are presented as median with first and third quartiles (Q1–Q3). A two-tailed p-value < 0.05 was considered statistically significant. Cohen's d was used as the primary effect size measure for pairwise comparisons, and eta-squared (η^2) was reported as a complementary measure. All statistical analyses and visualizations were performed using Python (version 3.11.5), with the assistance of the scipy, statsmodels, pandas, seaborn, and matplotlib libraries.

2.2. Patient Selection and Diagnostic Criteria

In this retrospective study, the institutional radiology database was retrospectively searched for patients who underwent brain MRI between November 2015 and September 2024 for evaluation of dural-based intracranial lesions. Patients with IDM or meningioma were classified using histopathological confirmation and clinical–radiological criteria. Histopathological diagnosis served as the reference when available. IDM was diagnosed without histopathological confirmation if there was a known systemic primary malignancy, the dural lesion was absent on prior MRIs, and there was interval development with progressive lesion growth consistent with metastatic disease. Meningioma was diagnosed in the absence of histopathological confirmation when no primary malignancy existed, the dural lesion exhibited typical imaging features, and stability in size and appearance was confirmed through follow-up MRIs. Patients were excluded for incomplete MRI exams, significant motion artifacts, or lesions with extensive hemorrhage or necrosis affecting reliable measurements. The study involved 56 patients: 18 with IDM (27 lesions) and 38 with meningiomas (single lesions each).

2.3. MRI Acquisition Protocol

All MRI examinations were performed using either a 1.5-T MRI scanner (Aera, Siemens Healthcare, Erlangen, Germany) equipped with an 18-channel head coil or a 3-T MRI scanner (Skyra, Siemens Healthcare) equipped with a 32-channel head coil. The routine brain tumor MRI protocol included non-enhanced conventional cranial MRI sequences, DSC perfusion imaging, and contrast-enhanced T1-weighted axial and coronal images following intravenous administration of a gadolinium-based contrast agent (0.1 mmol/kg). The contrast agent was injected at a rate of 3–5 mL/s,

 doi:10.20944/preprints202601.2266.v1

followed by a saline flush. DSC perfusion imaging was performed using a T2-weighted gradient-echo echo-planar imaging sequence*. A preload contrast dose was not administered, as preload administration may influence contrast leakage–related parameters, particularly percentage signal recovery (PSR).

2.4. Image Evaluation and Perfusion Analysis

All MRI examinations were independently reviewed and subsequently evaluated by consensus between two neuroradiologists with 12 and 5 years of experience in neuroradiology, respectively. Perfusion data were transferred to a dedicated workstation running commercially available software for DSC perfusion imaging analysis (syngo.via, Siemens Healthcare). Following evaluation of conventional MRI sequences, post-processing of DSC perfusion imaging data was performed. Time–signal intensity curves were generated for each lesion. An arterial input function was manually selected from the middle cerebral artery, and CBV and CBF maps were generated. Regions of interest (ROIs) were placed within the enhancing solid portion of each lesion, avoiding necrotic or hemorrhagic areas, with reference ROIs in contralateral normal-appearing white matter. From these ROIs, mean CBV and CBF values were recorded. Relative perfusion parameters (rCBV and rCBF) were calculated by normalizing lesion values to corresponding WM values.

Time–signal intensity curves were generated for both lesion and WM ROIs. Wash-in time was defined as the time interval from baseline to the point of maximal signal drop. Relative wash-in time (rWiT) was calculated as the ratio of lesion wash-in time to WM wash-in time.

PSR was calculated using the classical formula:

$$PSR = (S1 - Smin) / (S0 - Smin)$$

where S0 represents the baseline signal intensity before contrast administration, S min the minimum signal intensity at peak contrast-induced signal drop, and S1 the signal intensity measured at a predefined late time point (90 seconds after contrast injection). Relative PSR (rPSR) was obtained by normalizing lesion PSR values to those measured in the contralateral normal-appearing white matter.

The wash-outslope was defined as a quantitative measure of the rate of signal recovery following the first-pass contrast bolus and was calculated as:

$$\text{Wash-out slope} = (S1 - Smin) / (t1 - tmin)$$

where tmin corresponds to the time point at which the minimum signal intensity (Smin) occurs, and t1 represents the time point at which the late signal intensity (S1) was measured. This parameter reflects the speed of post-bolus signal recovery and provides complementary information to PSR regarding contrast leakage and vascular permeability characteristics of the lesion.

Mean ADC values were measured in diffusion-weighted sequences, with ROIs spatially corresponding to perfusion ROIs placed on the solid portion of each lesion.

Additionally, a subgroup analysis was conducted to compare breast cancer metastases in the IDM cohort with metastases originating from other primary tumors.

2.5. Machine Learning Models (LDA, L2 Logistic Regression, Linear SVM)

ML analysis were performed to differentiate Intradural Meningiomas (IDM) from meningiomas using parameters derived from perfusion MRI. Three models were assessed: Linear Discriminant Analysis (LDA), L2-regularized Logistic Regression, and Linear Support Vector Machine (Linear SVM). Patient-level grouped cross-validation was employed to prevent data leakage, with nested cross-validation for model training and evaluation. Evaluation utilized a 5-fold GroupKFold method for unbiased performance estimation and hyperparameter tuning, conducted through Optuna. The primary metric for evaluation was the area under the receiver operating characteristic curve (ROC), with models incorporating median imputation and feature standardization. Performance assessment was limited to outer test folds, resulting in ROC curves for performance stability analysis. Two feature sets were evaluated to understand the impact of model complexity on diagnostic

 doi:10.20944/preprints202601.2266.v1

performance: a reduced feature set with two parameters (rCBF_mean and rCBV_mean) selected for their statistical significance and clinical relevance, and an extended feature set with seven parameters (including ADC, wash-in time, PSR, wash-out slope, and gender) providing a more comprehensive analysis of perfusion, diffusion, and demographic factors. All three machine learning models were trained and evaluated separately using both feature sets under identical nested cross-validation and hyperparameter optimization procedures. Univariate analysis of perfusion biomarkers rCBF_mean and rCBV_mean was conducted alongside ML-based classification. ROC curve analysis, performed separately for each biomarker using lesion-level data, calculated the area under the curve (AUC) to assess their ability to distinguish between IDM and meningiomas. Out-of-fold (OOF) predicted probabilities from the outer folds were aggregated to construct overall ROC curves and to support clinically oriented decision threshold analyses. To adjust for within-patient correlations from multiple lesions, cluster-based bootstrap resampling was used to derive 95% confidence intervals for the AUCs. A clinically relevant threshold was chosen to ensure a minimum sensitivity of 85% for metastasis detection, with corresponding sensitivity and specificity values reported for each threshold. Machine learning analyses were implemented using Python (version 3.11.5) with scikit-learn and Optuna libraries.

3. Results

3.1. Patient and Lesion Characteristics

A total of 56 patients (mean age, 57.6 ± 11.2 years; 20 men) were included in the study. Among them, 18 patients had IDM, contributing a total of 27 IDM lesions, whereas 38 patients had meningiomas, with one lesion per patient, resulting in 38 meningioma lesions. Overall, 65 lesions were analyzed.

Among the IDM, the most common primary tumor origin was breast cancer (12 lesions, 44.4%), followed by GBM (7 lesions, 25.9%), colon cancer (3 lesions, 11.1%), lung cancer (2 lesions, 7.4%), and one lesion each from medulloblastoma, melanoma, and KML (3.7% each). The cohort consisted of 36 females (64.2%) and 20 males (35.8%) based on patient count.

3.2. Perfusion and Diffusion Parameters in IDM and Meningiomas

Relative perfusion parameters differed significantly between IDM and meningiomas. Median rCBV_mean was significantly higher in meningiomas compared with IDM (4.71 [IQR 3.71] vs. 2.95 [IQR 1.54], $p < 0.001$) (Figure 1).

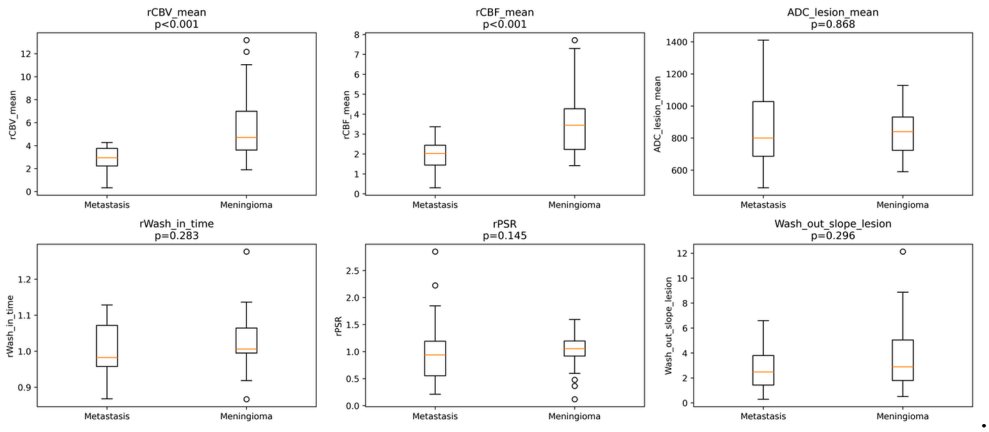

Figure 1. Perfusion, diffusion, and dynamic DSC parameters in dural metastases and meningiomas. Boxplots show the distribution of DSC-derived perfusion, diffusion, and dynamic parameters in dural metastases and meningiomas. rCBV_mean and rCBF_mean were significantly higher in meningiomas ($p < 0.001$), whereas ADC_lesion_mean, relative wash-in time (rWiT), relative percentage signal recovery (rPSR), and wash-out slope did not differ significantly between groups.

 doi:10.20944/preprints202601.2266.v1

Similarly, rCBF_mean values were markedly elevated in meningiomas (3.44 [IQR 2.11]) relative to IDM (2.02 [IQR 1.10], $p < 0.001$) (Table 1). Both rCBF_mean and rCBV_mean demonstrated large effect sizes (Cohen's d >1.1; $\eta^2 \approx 0.35$), indicating marked separation between groups. In contrast, no significant differences were observed between groups in terms of ADC_lesion_mean, rWiT, rPSR, or wash-out slope (Figure 1). Representative perfusion maps and time–signal intensity curves for intracranial dural metastasis and meningioma are shown in Figures 2 and 3.

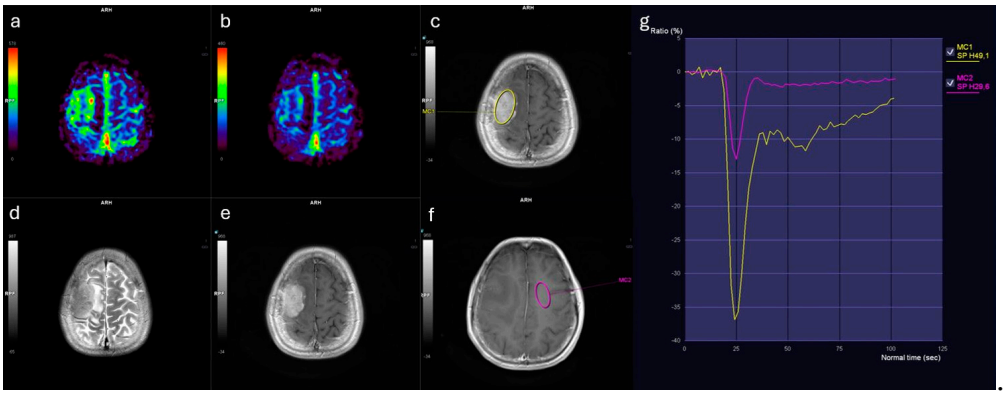

Figure 2. Brain MRI findings in a 42-year-old female with solitary intracranial dural metastasis from breast cancer. (a) Relative cerebral blood volume (rCBV) map shows mildly increased perfusion. (b) Relative cerebral blood flow (rCBF) map demonstrates corresponding flow increase. (c) Contrast-enhanced T1-weighted image with region of interest (ROI, yellow contour) placed within the enhancing lesion. (d) T2-weighted image reveals lesion morphology. (e) Contrast-enhanced T1-weighted image illustrates enhancement pattern. (f) Contrast-enhanced T1-weighted image with ROI in contralateral normal-appearing white matter (pink contour). (g) Time–signal intensity curves: lesion (yellow curve) shows altered contrast dynamics compared to white matter (pink curve).

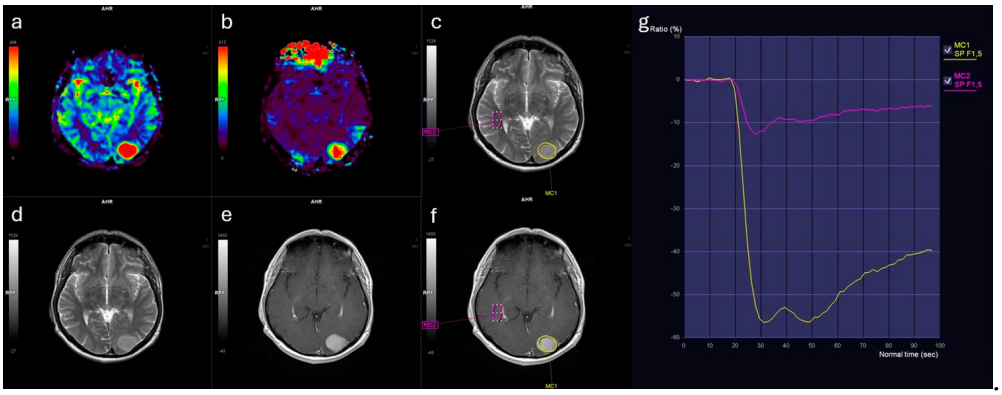

Figure 3. Brain MRI findings in a 52-year-old male with atypical meningioma (WHO Grade 2). (a) Relative cerebral blood volume (rCBV) map demonstrates markedly increased perfusion. (b) Relative cerebral blood flow (rCBF) map shows corresponding elevated flow. (c) T2-weighted image with region of interest (ROI, yellow contour) placed within the solid portion of the lesion. (d) T2-weighted image illustrates lesion morphology. (e) Contrast-enhanced T1-weighted image depicts homogeneous enhancement. (f) Contrast-enhanced T1-weighted image with ROI in contralateral normal-appearing white matter (pink contour). (g) Time–signal intensity curves: lesion (yellow curve) reveals higher perfusion and distinct kinetics compared to white matter (pink curve).

 doi:10.20944/preprints202601.2266.v1

Table 1. Comparison of perfusion, diffusion, and dynamic MRI parameters between dural metastases and meningiomas.

Parameter	Dural metastases (n=27) Median (Q1–Q3)	Meningiomas (n=38) Median (Q1–Q3)	Mann–Whitney U	p value
rCBV_mean	2.95 (2.22–3.75)	4.71 (3.61–6.99)	188	**<0.001**
rCBF_mean	2.02 (1.44–2.44)	3.44 (2.23–4.27)	184	**<0.001**
ADC_lesion_mean	800 (687–1027)	840 (723–931)	500	0.868
rWash_in_time	0.98 (0.96–1.07)	1.01 (0.99–1.06)	432	0.283
rPSR	0.94 (0.55–1.19)	1.05 (0.92–1.20)	403	0.145
Wash_out_slope_lesion	2.48 (1.43–3.79)	2.89 (1.79–5.05)	434	0.296
rCBV: relative Cerebral Blood Volume, rCBF: relative Cerebral Blood Flow, ADC: Apparent Diffusion Coefficient, rPSR: relative Percentage Signal Recovery,				

3.3. Subgroup Analysis of IDM According to Primary Tumor Origin

A subgroup analysis was performed within the IDM cohort to explore potential differences between breast cancer metastases (n = 12) and metastases from other primary tumors (n = 15). Within the IDM cohort, a subgroup analysis was performed to investigate potential differences between breast cancer metastases (n = 12) and metastases from other primary tumors (n = 15). No statistically significant differences were observed between these subgroups in rCBV_mean (p = 0.064), rCBF_mean (p = 0.407), ADC_lesion_mean (p = 0.380), rWiT (p = 0.241), rPSR (p = 0.242), or washout slope (p = 0.223).

3.4. Diagnostic Performance of Perfusion Biomarkers and Machine Learning Models

Univariate ROC analysis revealed statistically significant differences in both rCBF_mean and rCBV_mean between IDM and meningiomas. The AUC for rCBF_mean was 0.82 (95% CI, 0.72–0.90), and for rCBV_mean was 0.82 (95% CI, 0.73–0.91) (Figure 4). Using clinically oriented thresholds prioritizing metastasis detection (minimum sensitivity of 85%), rCBF_mean <2.9 and rCBV_mean <4.1 yielded metastasis sensitivities of 85%, with corresponding meningioma specificities of 61% and 66%, respectively.

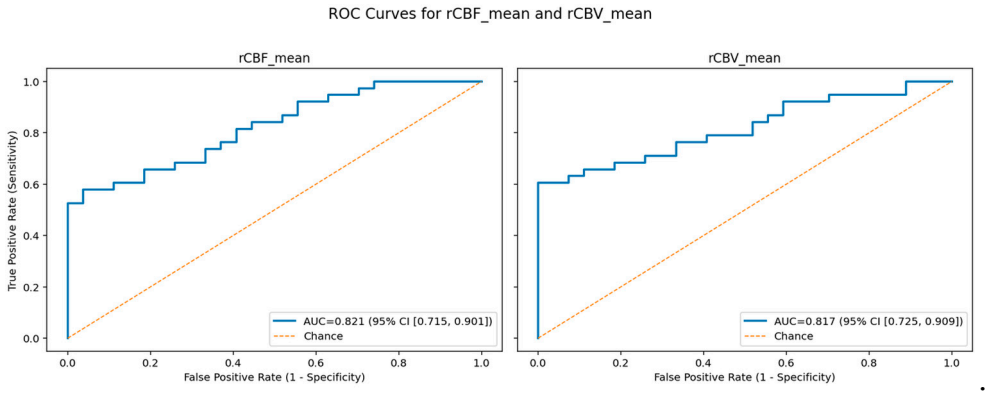

Figure 4. Univariate ROC curves for rCBF_mean and rCBV_mean. Receiver operating characteristic (ROC) curves illustrating the standalone diagnostic performance of rCBF_mean and rCBV_mean for differentiating

 doi:10.20944/preprints202601.2266.v1

dural metastases from meningiomas. Both parameters demonstrated strong discriminatory ability, with area under the curve (AUC) values of approximately 0.82.

When using a two-parameter feature set, LDA exhibited the best diagnostic performance, with an average fold-level AUC of approximately 0.85 and an OOF-AUC of 0.81, resulting in a Brier score of 0.17 (Figure 5). By maintaining metastasis sensitivity at 85% using a clinically focused decision threshold, the LDA model achieved 85% meningioma specificity, compared to 61% and 66% specificity obtained with rCBF_mean and rCBV_mean alone (Table 2). In contrast, L2-modulated Logistic Regression and Linear SVM achieved an average OOF-AUC of approximately 0.81 with the two-parameter feature set, but their performance decreased with the seven-parameter feature set (mean AUC of 0.79 and 0.80, respectively).

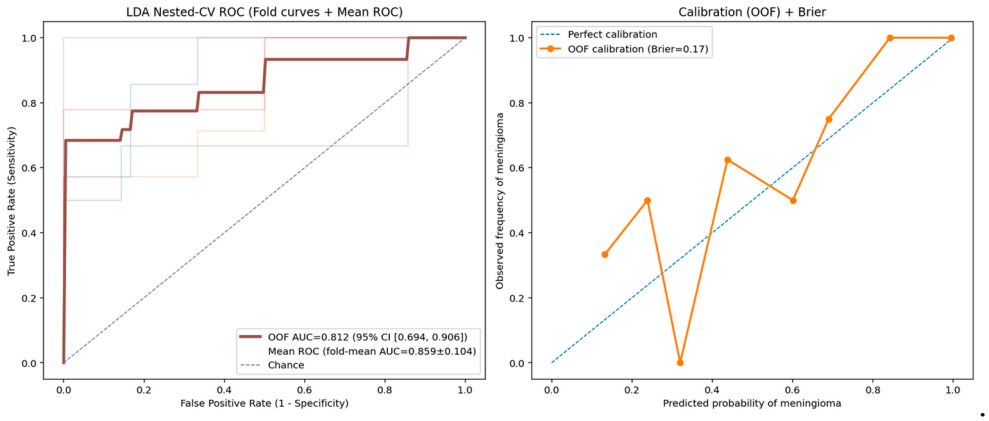

Figure 5. Nested cross-validated ROC and calibration of the LDA model. Receiver operating characteristic (ROC) curves obtained from patient-level grouped nested cross-validation for the linear discriminant analysis (LDA) model using rCBF_mean and rCBV_mean. The mean ROC curve and calibration plot based on out-of-fold predictions demonstrate stable discrimination and acceptable calibration performance.

Table 2. Diagnostic performance of single perfusion biomarkers and a multivariate LDA model in differentiating dural metastases from meningiomas.

Approach	**AUC (%95 CI)**	**Klinik threshold (metastasis sensitivity ≥0.85)**	**Metastasis Sensitivity**	**Meningioma Specificity**
Univariate rCBF_mean	0.82 (0.72–0.90)	2.88	0.85	0.61
Univariate rCBV_mean	0.82 (0.72–0.91)	0.72–0.90	0.85	0.66
Multivariate LDA model (rCBF_mean + rCBV_mean)	0.81 (0.72-0.89)	0.58 *(P(meningioma))*	0.85	0.85

rCBF: relative Cerebral Blood Flow , rCBV: relative Cerebral Blood Volume, LDA: Linear Discriminant Analysis, AUC: Area Under the Curve

4. Discussion

Meningioma is the most common meningeal tumor, often detected incidentally on MRI. Most are asymptomatic when small; however, larger tumors can cause neurological symptoms like headaches [5]. On a standard MRI, a typical metastasis and a typical meningioma show differently from a radiological standpoint. They appear as spherical or plaque-like formations extending along the dura mater, typically separated from brain parenchyma by a cerebrospinal fluid cleft. Characteristically, meningiomas exhibit intense and uniform contrast enhancement in 60–72% of

 doi:10.20944/preprints202601.2266.v1

cases, often associated with dural thickening known as the "dural tail" [9]. Calcifications occur in approximately 25% of cases [10], indicating slow growth and low malignancy [11], while 20% of patients show focal reactive hyperostosis [10,12]. Meningiomas can invade the dural sinus and adjacent bones, with nearly 50% accompanied by peritumoral edema [12]. They demonstrate high signal on DWI with low ADC values, suggesting high cellular density, though malignancy may lower ADC values further [13].

IDM presents with variable perivascular vasogenic edema and localized nodular dural thickening, often causing compression of brain parenchyma [13]. Post-contrast imaging reveals intense paramagnetic material accumulation, with hemorrhages and the "dural tail" phenomenon occurring in about half of cases. Enhanced dispersion is more common in IDM [7,14,15], and minimal ADC values indicate enhanced cellularity, but their correlation with histological types of metastasis remains debatable [16]. Metastases can exhibit either hypo- or hypervascular perfusion, largely hypervascular in cases from renal carcinoma, melanoma, and neuroendocrine carcinoma [17]. Distinguishing meningiomas from other conditions, such as IDMs, remains challenging, despite imaging advancements, complicating treatment decisions [17,18]. Approximately 2% of surgically removed dural masses initially diagnosed as meningiomas are actually mimic diseases, mostly metastases [9]. The incidence of IDM is difficult to determine, as it occurs in 8-9% of patients with extraneural malignancies and while about 20% of IDM cases are asymptomatic [14]. IDMs are responsive to systemic chemotherapy because they are located outside the blood-brain barrier, in contrast to parenchymal and leptomeningeal metastases [19]. As a result, preoperative distinction is required to choose the course of treatment in these situations

Our study evaluated the ability of DSC perfusion parameters and ML models to differentiate between IDM and meningiomas. The principal findings indicate that rCBF and rCBV serve as effective discriminators, with meningiomas showing notably higher values. While these univariate biomarkers alone offer good diagnostic accuracy (AUC ~0.82), a multivariate LDA model that combines both parameters delivered improved specificity at clinically relevant sensitivity. Other measures, like ADC and various dynamic contrast-enhanced metrics (rWiT, PSR, wash-out slope), did not provide significant additional discrimination in our sample. These findings highlight the complexity of perfusion-based differentiation and the potential for machine learning to translate this knowledge into a clinically useful tool.

Our finding that meningiomas have significantly higher rCBV and rCBF values than IDM is consistent with the understanding that meningiomas are highly vascular tumors. Angiomatous meningiomas exhibit higher CBV threshold values compared to fibroblastic and meningothelial types [6]. Anaplastic meningiomas are associated with elevated CBV thresholds and surrounding edema; however, the metastatic peritumoral area's CBV is lower due to tumor infiltration [20]. Intracranial meningiomas typically show an increased rCBV of 8.9, whereas various intracranial tumors reflect only modest increases, averaging 1.8 rCBV [21]. However, hypervascular intracranial tumors originating from conditions like melanoma can present high rCBV similar to meningiomas [22,23]. According to Hakyemez et al. [24], atypical meningiomas had a rCBV value of 12.25, whereas typical meningiomas at 6.63. In studies by Kremer et al. [6] and Furtner et al. [22], found that IDMs are less vascular than intracranial meningiomas, which is consistent with the results of our study. The rCBF and rCBV values on perfusion maps were comparable to those of meningiomas, according to studies by Fink and Fink [31] and Bendini et al. [32]. However, the diagnostic landscape is complicated by subsequent studies reporting divergent results. For instance, Lui et al. found no significant difference in rCBV between the two entities but identified a shorter normalized "relative wash-in time" in metastases [3]. The absence of significant differences in wash-in time, PSR, and wash-out slope in our cohort suggests that kinetic parameters may be more sensitive to methodological and cohort-related variability than steady-state perfusion metrics such as rCBV and rCBF.

More strikingly, our results contradict the study by Wu et al. , which found higher CBV and CBF in solitary IDM compared to meningiomas [5]. This inconsistency may arise from differences in tumor composition, histologic subtype distribution of meningiomas, normalization methods, and DSC

 doi:10.20944/preprints202601.2266.v1

protocols. Our finding of no perfusion difference between breast cancer IDM and metastases from other primaries suggests that, within our cohort, the primary origin was not a major confounder; however, this may not generalize. Despite the inconsistencies in the literature, the robust individual performance of rCBF and rCBV (AUC 0.82) in our cohort points to a solid diagnostic potential. To reflect the clinical priority of avoiding metastatic lesions, a clinically focused threshold of 85% for metastasis sensitivity was chosen. At this threshold, rCBF and rCBV provided specificity of 61% and 66%, respectively, while the LDA model using only these two parameters increased specificity to 85% while maintaining 85% sensitivity (Table 2). This represents a significant improvement in diagnostic confidence and potentially reduces the number of meningiomas mistakenly suspected of being metastases. The fact that the expanded feature set (including ADC, kinetic, and demographic data) did not improve performance suggests that rCBF and rCBV captured the baseline diagnostic signal in our data, and the addition of less discriminative variables only led to noise, indicating that rCBF and rCBV were sufficient to capture the baseline diagnostic signal.

Our study has several strengths, including the use of patient-level grouped nested cross-validation to prevent data leakage and provide robust performance estimates, rigorous bootstrap confidence intervals for univariate AUCs, and a deliberate clinical framing of results via sensitivity-prioritized thresholds. However, limitations must be acknowledged. The retrospective, single-center design and the modest sample size, particularly of the metastatic group limit generalizability. The inclusion of patients without histopathological confirmation, though based on stringent clinical-radiological criteria, is a potential source of limitation. The use of two different magnetic field strengths could introduce variance, although normalization to white matter should mitigate this effect. Future research should aim for prospective, multi-center validation in larger cohorts with uniform imaging protocols. Investigating the combination of DSC parameters with other non-invasive techniques, such as ASL as used by Furtner et al. [10]. The integration of radiomic features from perfusion maps or standard sequences might further enhance predictive power. Most importantly, future studies must carefully document and stratify results by the primary cancer type of metastases and the histological subtype of meningiomas to clarify the sources of heterogeneity observed across studies.

5. Conclusions

In conclusion, our study supports the role of DSC perfusion MRI, specifically rCBF and rCBV, as valuable biomarkers for differentiating IDM from meningiomas, with meningiomas showing higher perfusion in our cohort. The application of a simple linear ML model effectively synthesized this information, achieving an excellent balance of sensitivity and specificity that surpasses the use of either parameter alone. Despite ongoing contradictions in the literature, which likely reflect underlying pathological and technical diversity, a focused, clinically-guided analysis of perfusion data can provide significant diagnostic leverage. Integrating such models into the neuroradiological workflow has the potential to improve preoperative diagnostic confidence, thereby guiding more appropriate patient management.

Author Contributions: SE (Corresponding Author) – Conceptualization, Data Curation, Methodology, Writing – Original Draft, Software, Formal analysis, Resources, Supervision, Validation, Visualization, **HÖ** – Methodology, Formal Analysis, Visualization, Supervision, **AB** – Investigation, Validation, Data curation, **AA –** Validation, Resources, Investigation, **HC –** Formal analysis, Supervision, Methodology.

Funding: This research received no external funding.

Institutional Review Board Statement: The study was conducted in accordance with the Declaration of Helsinki and approved by the Selcuk University Faculty of Medicine Institutional Review Board (2024/541, date 2024-11-05).

 doi:10.20944/preprints202601.2266.v1

Informed Consent Statement: This retrospective study was approved by the Selcuk University Faculty of Medicine institutional review board (2024/541), and the requirement for informed consent was waived due to the retros-pective study design, in accordance with the Declaration of Helsinki.

Data Availability Statement: The data presented in this study are available on request from the corresponding author. The data are not publicly available due to privacy and ethical restrictions.

Conflicts of Interest: The authors declare no conflicts of interest.

Abbreviations

The following abbreviations are used in this manuscript:

IDM	Intracranial Dural Metastases
DSC	Dynamic Susceptibility Contrast
rCBV	relative Cerebral Blood Volume
rCBF	relative Cerebral Blood Flow
ADC	Apparent Diffusion Coefficient
ML	Machine Learning
PSR	Percentage Signal Recovery
ROIs	Regions of Interest
rWiT	relative Wash-in Time
LDA	Linear Discriminant Analysis
SVM	Support Vector Machine
ROC	Receiver Operating Characteristic Curve
AUC	Area Under the Curve
OOF	Out-of-Fold

References

1. Klingelhöfer, L.; Mucha, D.; Geiger, K.; Koch, R.; von Kummer, R. Prognostic Value of Conventional Magnetic Resonance Imaging for Adult Patients with Brain Tumors. *Clinical neuroradiology* **2015**, *25*, 281-289, doi:10.1007/s00062-014-0309-3.
2. Zakhari, N.; Torres, C.; Castillo, M.; Nguyen, T.B. Uncommon Cranial Meningioma: Key Imaging Features on Conventional and Advanced Imaging. *Clinical neuroradiology* **2017**, *27*, 135-144, doi:10.1007/s00062-017-0583-y.
3. Lui, Y.W.; Malhotra, A.; Farinhas, J.M.; Dasari, S.B.; Weidenheim, K.; Freeman, K.; LaSala, P.A. Dynamic perfusion MRI characteristics of dural metastases and meningiomas: a pilot study characterizing the first-pass wash-in phase beyond relative cerebral blood volume. *AJR. American journal of roentgenology* **2011**, *196*, 886-890, doi:10.2214/ajr.10.5309.
4. Galldiks, N.; Angenstein, F.; Werner, J.M.; Bauer, E.K.; Gutsche, R.; Fink, G.R.; Langen, K.J.; Lohmann, P. Use of advanced neuroimaging and artificial intelligence in meningiomas. *Brain pathology (Zurich, Switzerland)* **2022**, *32*, e13015, doi:10.1111/bpa.13015.
5. Wu, H.; Beylerli, O.; Gareev, I.; Beilerli, A.; Ilyasova, T.; Talybov, R.; Sufianov, A.; Guo, X. Are there reliable multiparametric MRI criteria for differential diagnosis between intracranial meningiomas and solitary intracranial dural metastases? *Oncology letters* **2023**, *26*, 350, doi:10.3892/ol.2023.13936.
6. Kremer, S.; Grand, S.; Rémy, C.; Pasquier, B.; Benabid, A.L.; Bracard, S.; Le Bas, J.F. Contribution of dynamic contrast MR imaging to the differentiation between dural metastasis and meningioma. *Neuroradiology* **2004**, *46*, 642-648, doi:10.1007/s00234-004-1194-2.
7. Kremer, S.; Grand, S.; Remy, C.; Esteve, F.; Lefournier, V.; Pasquier, B.; Hoffmann, D.; Benabid, A.L.; Le Bas, J.F. Cerebral blood volume mapping by MR imaging in the initial evaluation of brain tumors. *Journal of neuroradiology = Journal de neuroradiologie* **2002**, *29*, 105-113.
8. Hayashida, Y.; Hirai, T.; Morishita, S.; Kitajima, M.; Murakami, R.; Korogi, Y.; Makino, K.; Nakamura, H.; Ikushima, I.; Yamura, M.; et al. Diffusion-weighted imaging of metastatic brain tumors: comparison with histologic type and tumor cellularity. *AJNR. American journal of neuroradiology* **2006**, *27*, 1419-1425.

9. Louis, D.N.; Perry, A.; Wesseling, P.; Brat, D.J.; Cree, I.A.; Figarella-Branger, D.; Hawkins, C.; Ng, H.K.; Pfister, S.M.; Reifenberger, G.; et al. The 2021 WHO Classification of Tumors of the Central Nervous System: a summary. *Neuro-oncology* **2021**, *23*, 1231-1251, doi:10.1093/neuonc/noab106.
10. Boulagnon-Rombi, C.; Fleury, C.; Fichel, C.; Lefour, S.; Marchal Bressenot, A.; Gauchotte, G. Immunohistochemical Approach to the Differential Diagnosis of Meningiomas and Their Mimics. *Journal of neuropathology and experimental neurology* **2017**, *76*, 289-298, doi:10.1093/jnen/nlx008.
11. Shibuya, M. Pathology and molecular genetics of meningioma: recent advances. *Neurologia medico-chirurgica* **2015**, *55*, 14-27, doi:10.2176/nmc.ra.2014-0233.
12. Zeng, L.; Liang, P.; Jiao, J.; Chen, J.; Lei, T. Will an Asymptomatic Meningioma Grow or Not Grow? A Meta-analysis. *Journal of neurological surgery. Part A, Central European neurosurgery* **2015**, *76*, 341-347, doi:10.1055/s-0034-1543959.
13. Talybov, R.; Beylerli, O.; Mochalov, V.; Prokopenko, A.; Ilyasova, T.; Trofimova, T.; Sufianov, A.; Guang, Y. Multiparametric MR Imaging Features of Primary CNS Lymphomas. *Frontiers in surgery* **2022**, *9*, 887249, doi:10.3389/fsurg.2022.887249.
14. Laigle-Donadey, F.; Taillibert, S.; Mokhtari, K.; Hildebrand, J.; Delattre, J.Y. Dural metastases. *Journal of neuro-oncology* **2005**, *75*, 57-61, doi:10.1007/s11060-004-8098-1.
15. Lyndon, D.; Lansley, J.A.; Evanson, J.; Krishnan, A.S. Dural masses: meningiomas and their mimics. *Insights into imaging* **2019**, *10*, 11, doi:10.1186/s13244-019-0697-7.
16. Wallace, E.W. The dural tail sign. *Radiology* **2004**, *233*, 56-57, doi:10.1148/radiol.2331021332.
17. Tagle, P.; Villanueva, P.; Torrealba, G.; Huete, I. Intracranial metastasis or meningioma? An uncommon clinical diagnostic dilemma. *Surgical neurology* **2002**, *58*, 241-245, doi:10.1016/s0090-3019(02)00831-5.
18. Laidlaw, J.D.; Kumar, A.; Chan, A. Dural metastases mimicking meningioma. Case report and review of the literature. *Journal of clinical neuroscience : official journal of the Neurosurgical Society of Australasia* **2004**, *11*, 780-783, doi:10.1016/j.jocn.2004.03.001.
19. Zimny, A.; Sasiadek, M. Contribution of perfusion-weighted magnetic resonance imaging in the differentiation of meningiomas and other extra-axial tumors: case reports and literature review. *Journal of neuro-oncology* **2011**, *103*, 777-783, doi:10.1007/s11060-010-0445-9.
20. Marciscano, A.E.; Stemmer-Rachamimov, A.O.; Niemierko, A.; Larvie, M.; Curry, W.T.; Barker, F.G., 2nd; Martuza, R.L.; McGuone, D.; Oh, K.S.; Loeffler, J.S.; et al. Benign meningiomas (WHO Grade I) with atypical histological features: correlation of histopathological features with clinical outcomes. *Journal of neurosurgery* **2016**, *124*, 106-114, doi:10.3171/2015.1.Jns142228.
21. Toh, C.H.; Wei, K.C.; Chang, C.N.; Peng, Y.W.; Ng, S.H.; Wong, H.F.; Lin, C.P. Assessment of angiographic vascularity of meningiomas with dynamic susceptibility contrast-enhanced perfusion-weighted imaging and diffusion tensor imaging. *AJNR. American journal of neuroradiology* **2014**, *35*, 263-269, doi:10.3174/ajnr.A3651.
22. Furtner, J.; Oth, I.; Schöpf, V.; Nenning, K.H.; Asenbaum, U.; Wöhrer, A.; Woitek, R.; Widhalm, G.; Kiesel, B.; Berghoff, A.S.; et al. Noninvasive Differentiation of Meningiomas and Dural Metastases Using Intratumoral Vascularity Obtained by Arterial Spin Labeling. *Clinical neuroradiology* **2020**, *30*, 599-605, doi:10.1007/s00062-019-00808-x.
23. Nayak, L.; Abrey, L.E.; Iwamoto, F.M. Intracranial dural metastases. *Cancer* **2009**, *115*, 1947-1953, doi:10.1002/cncr.24203.
24. Hakyemez, B.; Erdogan, C.; Bolca, N.; Yildirim, N.; Gokalp, G.; Parlak, M. Evaluation of different cerebral mass lesions by perfusion-weighted MR imaging. *Journal of magnetic resonance imaging : JMRI* **2006**, *24*, 817-824, doi:10.1002/jmri.20707.